Al-Mustansiriyah Journal of Science
ISSN: 1814-635X (print), ISSN:2521-3520 (online) Volume 33, Issue 4, 2022 DOI: http://doi.org/10.23851/mjs.v33i4.1208

Research Article Open Access

Green Synthesis of A-Fe_2O_3 from Ginger Extract Enhanced the Potential Antioxidant Activity Against DPPH

Duoaa H. Hilo*, Ahmad H. Ismail, Zahraa S. Al-Garawi

Department of Chemistry, College of Science, Mustansiriyah University, Baghdad, IRAQ.

*Correspondent contact: duoaa1992@uomustansiriyah.edu.iq

Article Info

Received
17/08/2022

Accepted
02/10/2022

Published
30/12/2022

ABSTRACT

The synthesis of nanooxides in an easy and environmentally friendly way using simple and green materials is one of the hot topics of sustainable chemistry for many pharmaceutical and medical applications. Herein, we successfully synthesized α-Fe_2O_3 NPs (α-Fe_2O_3 NPs) using ginger extract. The prepared α-Fe_2O_3 NPs were examined using ultraviolet-visible reflection spectroscopy (UV-VIS), Fourier Transform Infrared Spectroscopy (FTIR), photoluminescence spectroscopy (PL), X-ray diffraction (XRD), field emission scanning microscopy (FE-SEM), energy-dispersive X-ray (EDX) spectroscopy, and zeta potential. After well characterizations, the potency of the prepared α-Fe_2O_3 NPs to monitor some scavenging activity was explored against DPPH. The results revealed that the intensity of the PL has one peak in the UV region between (480-490) nm of the spectrum depending on the geometric shape and size of the α-Fe_2O_3 NPS. The UV-visible spectra showed a peak at 296.0 nm, which represented the α-Fe_2O_3 NPs. The EDX micrograph confirmed pure oxide and the XRD pattern showed that the α-Fe_2O_3 NPs had an average crystal size (19.3) nm. SEM images of α-Fe_2O_3 NPs revealed irregular, rod, and spherical shapes and sizes ranging from (15 to 60) nm. Furthermore, the antioxidant activity of α-Fe_2O_3 NPs against DPPH showed 51.8% free radical scavenging ability at 360 µg/mL, which approved good evidence of the antioxidant activity of α-Fe_2O_3 NPs.

KEYWORDS: α-Fe_2O_3 NPs; green synthesis; ginger extract; antioxidant.

الخلاصة

يعد تصنيع الأكاسيد النانوية بطريقة سهلة وصديقة للبيئة باستخدام مواد بسيطة وامنة أحد اهم الاهتمامات الساخنة في مجال الكيمياء المستدامة والتي تحتمل العديد من التطبيقات الصيدلانية والطبية. تم في هذه الدراسة تحضير ناجح جزيئات الحديد النانوية (α-Fe_2O_3 NPs) باستخدام مستخلص نبات الزنجبي. تم توصيف الجسيمات النانوية المحضرة بالتحليل الطيفي للانعكاس المرئي فوق البنفسجي، مطياف فورييه للأشعة تحت الحمراء، مطيافية اللمعان الضوئي، حيود الأشعة السينية، الفحص المجهري لمسح الانبعاث الميداني، مطيافية الأشعة السينية المشتتة للطاقة، وجهد زيتا. بعد التوصيف الجيد للجسيمات النانوية، تم استكشاف فاعلية الجسيمات النانوية α-Fe_2O_3 المحضرة لكسح نشاط الجذور الحرة الناتجة من المركب DPPH. أوضحت النتائج أن شدة اللمعان الضوئي لها قمة واحدة في منطقة الأشعة فوق البنفسجية بين (480-490) نانومتر من الطيف اعتمادًا على الشكل الهندسي وحجم الجسيمات النانوية، كما وأظهرت الأطياف المرئية للأشعة فوق البنفسجية قمة واحدة ايضا عند طول موجي 296. نانومتر، والتي تمثل وجود الجسيمات النانوية، في حين أكدت الصورة المجهرية لمسح الانبعاث الميداني وجود أوكسيد واحد نقي وأظهر نمط حيود الاشعة السينية أن جسيمات الحديد α-Fe_2O_3 NPs لها متوسط حجم بلوري (19.3) نانومتر وكشفت صور الماسح الالكتروني ان الاجسام النانوية لأوكسيد الحديد لها أشكال وأحجام كروية وقضيبية وغير منتظمة تتراوح من (15 إلى 60) نانومتر. علاوة على ذلك، أظهرت تلك الجسيمات النانوية المحضرة هنا نشاطا مضادا للأكسدة ضد الجذور الحرة المتولدة من DPPH مما يدل على قدرتها على تنظيف الجذور الحرة بنسبة 51.8 ٪ عند 360 ميكروغرام/مل.

INTRODUCTION

Metal oxide-based NPs are synthesized to modify the properties of their corresponding metal-based NPs. In the presence of oxygen, iron (Fe) NPs instantly oxidize to iron oxide (α-Fe_2O_3), increasing their reactivity compared to iron NPs. Metal oxide NPs are made primarily for their increased reactivity and efficiency [1]. Because of their superior physicochemical properties when compared to bulk counterparts, iron oxide NPs have gained popularity in recent years. Because of their chemical stability and low cost among transition metal oxides, iron oxide NPs have piqued the interest of researchers over the last decade. Iron oxide can be found in nature in a variety of forms, including FeO, αFe_2O_3, β-Fe_2O_3, γ-Fe_2O_3, and

Fe_3O_4 [2]. Because of its unique electrical, optical, and magnetic properties, interest in the synthesis of iron oxide NPs has grown over the last few decades. Iron is, indeed, the central focus of modern materials science [3]. Iron oxide NPs (IO NPs) are non-toxic [4] and biocompatible with superior magnetic properties that allow wide-ranging applications in biomedicine such as hyperthermia, photoablation therapy, biosensors, and physiotherapy applications [5]. They can also be used for magnetic particle imaging (MPI), magnetic resonance imaging (MRI), drug administration with precision, proteins, antibodies, and nucleic acids, tissue repair, and separation of biomolecules [6], and antimicrobial agents [7].

Furthermore, magnetic NPs have the ability to control biomolecule motion and transport, as well as generate heat in an external magnetic field to kill tumor cells. The biocompatibility of αFe_2O_3 and γ-Fe_2O_3 is a significant advantage, and ferumoxytol (Feraheme) was approved by the US Food and Drug Administration in 2009 for the treatment of patients with chronic kidney disease who are iron deficient [8]. In general, it absorbs photons at wavelengths as long as 600 nm in general and collects more than 40% of the solar light spectrum. Its color is red because of these abilities. Its narrow bandgap of about 2.0-2.2 eV makes it a promising photocatalysis candidate. [9].

Recently, there has been a general trend toward the use of NPs in biomedical applications. Among the interesting properties of superparamagnetic IO NPs, they are low toxic and therefore they are used in many fields in diagnostic, therapeutic, or prognostic fields, including hyperthermia, drug delivery, magnetic resonance imaging, and cell separation. Zinc oxide, silver, gold, and core-shell silver-gold NPs have previously showed anti-diabetic properties. Furthermore, Sharifi *et al.* discovered that these superparamagnetic IO NPs suppress the vast majority of risk genes involved in the development of T2DM in human primary adipocytes [10]. These NPs showed significant antioxidant activity [11]. Antioxidants are substances in the body that fight free radicals and prevent or slow down cell damage caused by free radicals and unstable molecules. Antioxidants can control autoxidation by interrupting free radical propagation or inhibiting free radical formation, reducing oxidative stress, improving immune function, and increasing healthy longevity. Antioxidants are found in many foods, including fruits and vegetables, and are also available as dietary supplements [12,13].

In this research, IO NPs were synthesized by a green method using ginger plant extract. The resulting NPs were well characterized by UV, FTIR, X-ray diffraction, SEM, AFM, and zeta potential. The antioxidant potential against DPPH has been investigated compared to that of vit C.

MATERIALS AND METHODS

Chemicals and reagents

Iron Sulfate heptahydrate ($FeSO_4.7H_2O$) (BDH), Sodium hydroxide (NaOH) Sigma-Aldrich It was received from the chemical materials store at the College of Science, Mustansiriyah University. The extract was made in the lab with dried ginger and all solutions were made with deionized water. To study the antioxidant activity, 2,2-diphenyl- 1-picrylhydrazyl (DPPH) was used against Vit C as a standard antioxidant.

Preparation of the extract

The dried ginger was purchased from the local market, washed well with distilled water several times, dried, ground, and kept in an airtight container afterward before analysis. A weight of 10 g of ginger rhizome was mixed with 200 ml of deionized water and boiled at 80 °C for 15 minutes until a yellow solution remained. After being cooled to room temperature, the solution was filtered to obtain a clear yellow plant extract solution. This plant extract was used as a reducing agent. The filter extract was further used for the green synthesis of α-Fe_2O_3 NPs.

Green Synthesis of Fe_2O_3 NPs

A weight of 3 g of Iron Sulfate heptahydrate ($FeSO_4.7H_2O$) was dissolved in 300 mL deionized water for a final concentration of 0.1 M. To achieve a homogeneous solution, the solution was agitated at room temperature for 5 minutes. Then, 20 ml of rhizome extract was added with stirring until the solution turned yellow. After 30 minutes of stirring, 1 M NaOH was dropped wise until the blue solution turned into grey. The solution was centrifuged at 7500 rpm for 10 minutes and the supernatant was rinsed multiple times with water. A black-reddish α-Fe_2O_3 NPs were collected and dried at 95°C for 4 hours. The dried α-Fe_2O_3 NPs were calcined at 400°C for 4 hours to remove any evaporable impurities. The calcined samples were cooled to room temperature and kept for future research [14].

ISSN: 1814-635X (print), ISSN:2521-3520 (online) Volume 33, Issue 4, 2022 DOI: http://doi.org/10.23851/mjs.v33i4.1208

Characterization of α-Fe_2O_3 NPs

For optical studies, UV-vis 1800 spectrophotometer (Shimadzu, Japan) with a wavelength range from 210 to 800 nm. Poly(l-methyl) (PL) was used for UV- analysis to provide valuable information about the purity and quality of the material. α-Fe_2O_3 NPs were further characterized using FTIR spectroscopy, XRD, AFM, EDX, and SEM and zeta potentia (ζ-potential).

RESULTS AND DISCUSSION

UV–visible spectroscopy analysis

UV-vis spectroscopy was used to confirm the synthesis of α-Fe_2O_3 NPs. Due to the surface plasmon resonance (SPR) effect, the conducting electrons begin to oscillate at a specific wavelength range, as shown in Figure 1. The presence of α-Fe_2O_3 NPs demonstrated by the presence of a peak at 296.0 nm, which represents the UV-visible spectra of prepared α-Fe_2O_3 NPs. This result was consistent with the findings of Paulson, E and Jothibas, M [15].

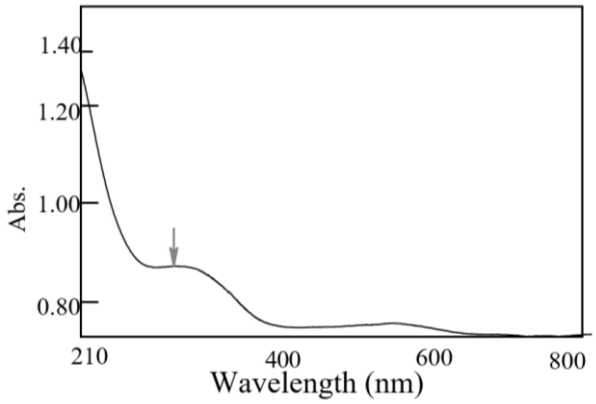

Figure 1. UV-vis spectrum of α-Fe2O3 NPs synthesized by Zingiber extract.

FTIR spectroscopy

FTIR spectrum of α-Fe_2O_3 NPs synthesized by Zingiber is shown in Figure 2. Several peaks at 3398 cm^{-1} appeared due to the a broad-OH of phenolic compounds. A strong peak at 1604 cm^{-1} indicated the involvement of amide C=O extension, in the reduction process. Also, the presence of a peak at 2956 cm^{-1} assigned for O = C = O stretching of carbon dioxide. The strong peaks at 1487 and 1293 cm^{-1} showed the alkane's CH bending and the sulfide group' S=O stretching, respectively. Peaks at 748 and 576 cm^{-1} verified the presence of NPs. These peaks were due to the organic compounds of ginger extract that play an important role in reducing and stabilizing α-Fe_2O_3 NPs, this result was in agreement with Abdulah *at el* [16].

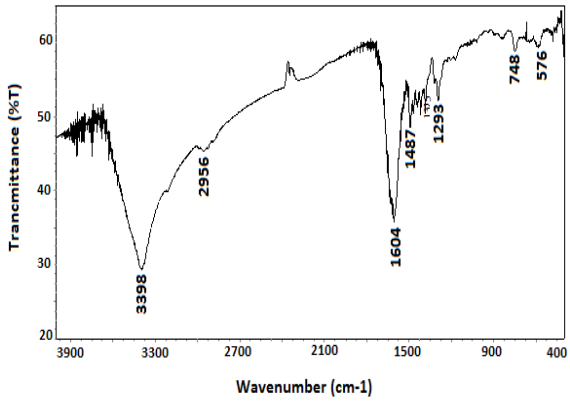

Figure 2. FTIR spectrum of α-Fe2O3 NPs.

Photoluminescence (PL) spectroscopy

For crystalline quality, the photoluminescence (PL) technique was used. All spectra were composed of one emanation peak, Figure 3. A peak in the region (480-490 nm) indicated the emission peak of the photoluminescence analysis of α-Fe_2O_3 at room temperature and the formation of iron oxide NPs [17].

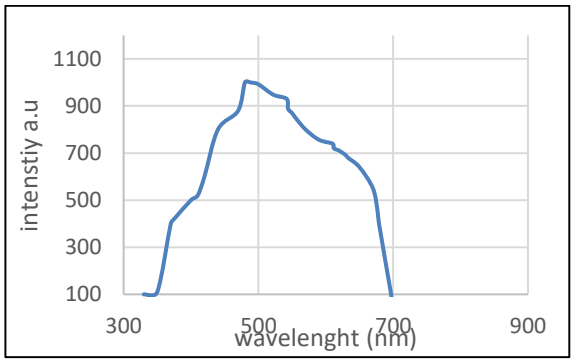

Figure 3. PL spectra of the α-Fe2O3 NPs prepared from Zingiber extract.

Energy gap values of α-Fe_2O_3 NPs measured according to the equation [18]:

$$Eg\ (eV) = 1240/x \quad (1)$$

Where Eg is the energy gap, and x is the maximum wavelength represents the value of the energy gap (2.5 eV) at the wavelength (485 nm).

X-ray diffraction (XRD)

X-ray crystallographic study was performed to confirm the crystalline structure of α-Fe_2O_3 NPs after calcination at 400 °C. The analysis was carried out by a Shimadzu-7000 Powder X-Ray diffractometer with Cu-Kα (λ=1.54 Å) radiation in a range from 10 to 70 A˚. The Debye-Sherrer equation was used to calculate the particle size [19].

$$D = K*\lambda/\beta*Cos(\theta) \quad (2)$$

Where D is the size of the crystallite, K=0.9 Sherrer constant, λ is the X-ray wavelength, β is the full width half maximum (FWHM) and θ is the Braggs diffraction angle. XRD patterns of α-Fe_2O_3 NPs are observed at 2θ= 24.36˚, 33.25˚, 35.76 ˚, 41.02 ˚, 43.27 ˚, 49.43 ˚, 54.19 ˚, 57.22, ˚ and 64.22. The corresponding reflecting planes are (012), (104), (110), (113), (116), (018), (214), (300), respectively. The formation of α-Fe_2O_3 NPs indexed of JCPDS No. 33-0664. The analysis also revealed that the synthesized NPs were crystalline. The average crystal size was (19.3) nm, which was calculated using Debye-Sherrer equation.

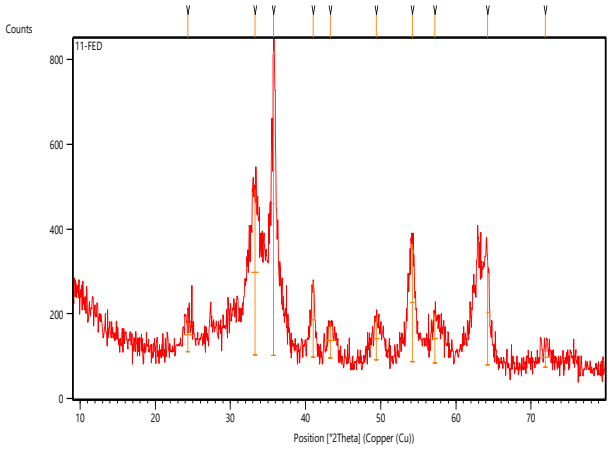

Figure 4. X-ray diffraction pattern of α-Fe_2O_3 NPs powder.

The sharp diffraction peaks indicated the crystallinity of the preparation material, see Figure 4. Particles size was calculated to be (19.3) nm, in agreement with Huang, Wei, et al [20], and Samrot, Antony V, et al [21].

Scanning electron microscopy (SEM)

The morphology, shape, and size of the synthesized green NPs were effectively illustrated using SEM micrographs. SEM scans of α-Fe_2O_3 NPs indicated that they were spherical, rod-shaped, and irregular in form, with sizes ranging from 15 to 60 nm, Figure 5. This size range also corroborated the particle size determined by the XRD spectra in Figure 4. The aggregation in the SEM images was most likely caused by electrostatic contact between the NPS surface layers [22]. A similar observation was reported earlier by Saqib, Saddam, *et al* [23].

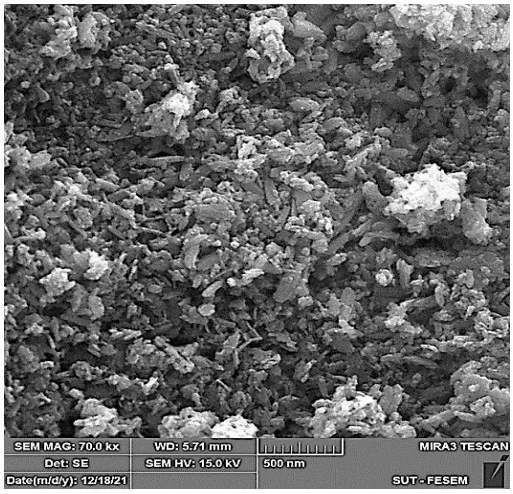

Figure 5. SEM analysis of α-Fe_2O_3 NPs.

Energy dispersive–X-ray (EDX)

The initial composition of α-Fe_2O_3 NPs was determined by EDX Figure 6. The weight percentage was 24.1% and 75.9% for oxygen and iron, respectively. The presence of iron and oxygen peaks suggested that iron oxide NPs were formed, a similar observation reported earlier by Ali, Musrat *et al* [24].

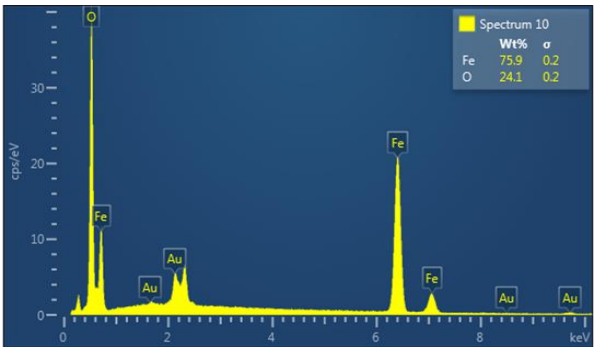

Figure 6. EDX spectrum of α-Fe_2O_3 O NPs.

Table 1 showed that the practical EDX values were compatible with the calculated values, obtained by x-ray mapping.

Table 1. Practical and Calculated ratio of α-Fe_2O_3.

Experimental formula	Fe%	O%
a-Fe_2O_3	75.86 (70.1)	24.14 (30.1)

Atomic Force Microscopy (AFM)

AFM (spm-AA300 contact mode spectrometer, Angstrom) was used to characterize the size and morphology of α-Fe_2O_3 NPs. The origin of the surface morphology of the irregularly shaped particle sizes and the size distribution broadens of α-Fe_2O_3 NPs synthesized by ginger extract are shown in Figure 7.

The images confirmed the uniform distribution of α-Fe_2O_3 NPS, as did the majority of NPs (aged for 2 weeks) were approximately 30–100 nm. The size obtained in this study almost agreed with other studies by Jin Ying *et al* [25].

Transmission Electron Microscopy (TEM)

Imaging by TEM was useful for confirming the size and shape of the green synthesized produced iron oxide NPs as shown in Figure 8 at different scale bars (a and b). There were clusters of NPs dispersed during the formation of the hematite. The particle sizes of hematite α-Fe_2O_3 NPs were (20–40 nm) with an average size of 25 nm, which confirmed the results predicted by XRD analysis using Debye-Scherrer formula. This result agreed with the study of Pallela, Panduranga Naga Ummey *et al* [26], where iron oxides NPS were synthesized by Sida cordifolia plant extract.

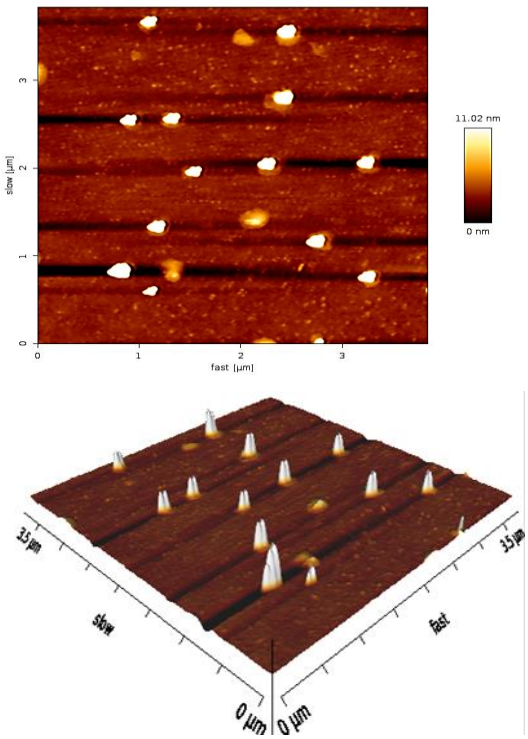

Figure 7. AFM microscope shows the distribution and roughness of of α-Fe_2O_3 NPs.

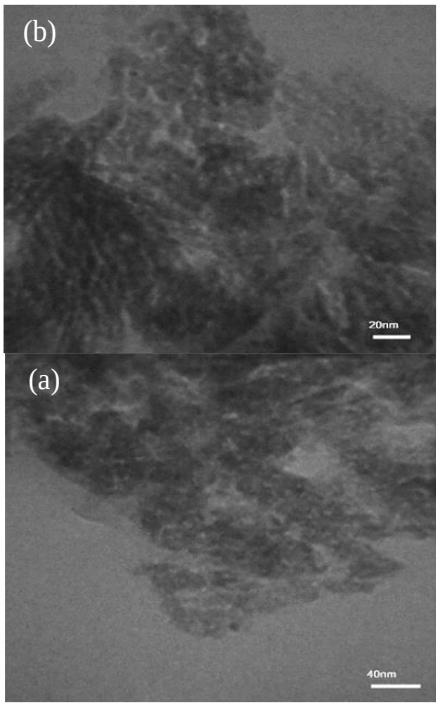

Figure 8. TEM images of the green synthesized iron oxide NPs. a) IO NPs at a scale bar 40nm, b) IONPs at a scale bar 20nm.

Zeta potential analysis (ζ-potential)

The zeta potential (ζ-potential) analysis was important for studying the net charge on the surface of NPs and calculating the charge to understand their stability. The potential value of α-Fe_2O_3 NPS was observed to be 13.8 mV (see Figure 9) which indicated high stability of NPs. The presence of ζ-potential values within the positive range only demonstrated that the surface of the particles prepared from α-Fe_2O_3 within the nanocomposite was homogeneous (i.e a charged surface of one type). Although the positive charge value was small, the prepared particles were agglomerated and reduced the surface area [27].

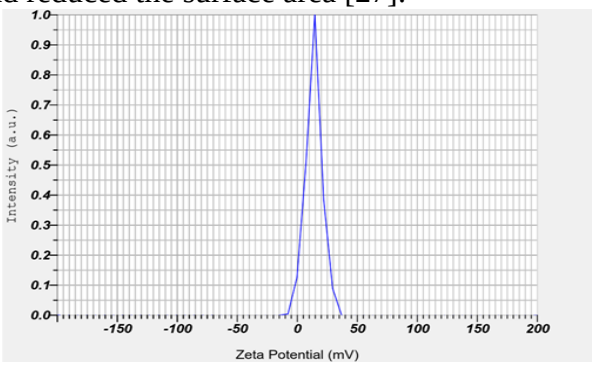

Figure 9. zeta potential for α-Fe_2O_3 NPs.

Antioxidant Activity

Dietary antioxidants are the first line of defense against free radicals [13]. IC50 value assists the estimation of the material amount able to inhibit 50% of DPPH. The lower the IC50 value, the greater the scavenging potency. The present results showed the scavenging activity for dried ginger compared with Vitamin C as a standard.

Vitamin C exhibited powerful antiradical activity against DPPH with IC50=23 µg/mL, Figure 10 and Table 2.

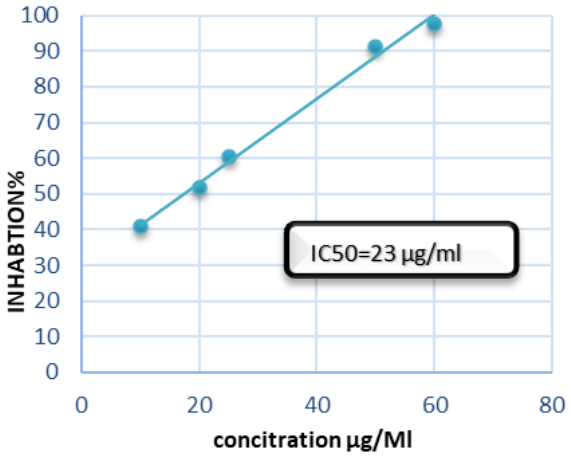

Figure 10. Vitamin C antiradical inhibition plot against DPPH.

Table 2. Vitamin C inhibitory percentage on DPPH.

Concentration µg/mL	Inhibition %
10	40.8
20	51.66
25	60.6
50	91.3
60	97.6

The scavenging power of α-Fe_2O_3 NPS showed good inhibitory characteristics against DPPH with IC50 = 312.11 µg/mL, Figure 11. The inhibition activity of α-Fe_2O_3 NPs was close to that of vitamin C. By increasing the concentration of NPs, the antioxidant activity was increased [28].

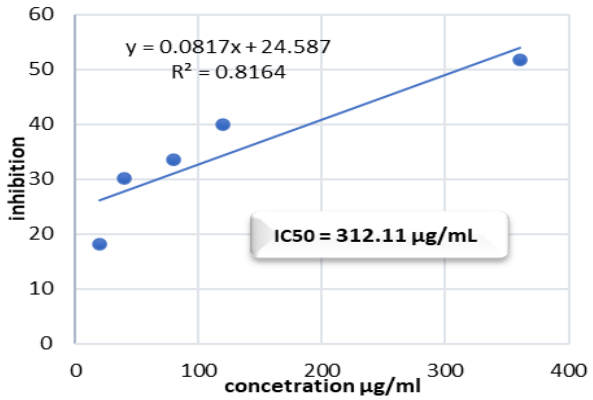

Figure 11. α-Fe_2O_3 NPs antiradical inhibition plot against DPPH.

Results showed that the highest scavenging % was at 360 ppm of α-Fe_2O_3 NPs with 51.8% (see Table 3), indicated good antioxidant activity. This result was in agreement with Ahmad *at el* [29,30]. This IC50 value of the prepared α-Fe_2O_3 NPs was lower than that previously prepared from the natural biowaste precursor, namely Psidium guajava leaves (579.9 µg/ml) [31], which indicated stronger inhibitory effect. However, This IC50 value was higher than that of α-Fe_2O_3 NPs prepared by Centaurea alba extract (287 µg/mL) Jian Xiu *et al* [31].

Table 3. The α-Fe_2O_3 NPS inhibitory percentage against DPPH.

Concentration µg/mL	Inhibition %
10	12
20	18.1
40	30.2
80	33.5
120	40
360	51.8

CONCLUSIONS

We have demonstrated here successful use of a natural and low-costed reducing agent to prepare metallic oxide nanostructures, the ginger plant extract. The green synthesis of NPs here helped in avoiding organic solvents and hazardous and toxic waste. The Uv-vis results confirmed the surface plasmon resonance of the biosynthetic iron oxide. The biocombined NPs using ginger extract demonstrated good catalytic activity. The potential value of α-Fe_2O_3 NPS (13.8 mV) indicated the stability of these NPs. Furthermore, the current study provided good evidence for the antioxidant activity of the green-synthesized α-Fe_2O_3 NPs against DPPH.

ACKNOWLEDGMENT

The authors would like to thank Mustansiriyah University in Baghdad, Iraq (www.uomustansiriyah.edu.iq) for their assistance with this project.

Disclosure and conflicts of interest: The authors declare that they have no conflicts of interest.

REFERENCES

[1] Razak, K. Abdul, N. Mohamad Nor, and Nur Syafinaz Ridhuan. 'Metal Oxide Nanostructure-modified Electrode for Glucose Biosensor.' Advanced Materials and their Applications: Micro to nanoscale, One Central Press (OCP), United Kingdom (2017): 31-68.."

[2] Sharma et al. Capping agent-induced variation of physicochemical and biological properties of α-Fe2O3 NPs.' Materials Chemistry and Physics 258 (2021): 123899.." https://doi.org/10.1016/j.matchemphys.2020.123899
[3] M. A. Ansari and S. M. M. Asiri, "Green synthesis, antimicrobial, antibiofilm and antitumor activities of superparamagnetic γ-Fe2O3 NPs and their molecular docking study with cell wall mannoproteins and peptidoglycan," Int. J. Biol. Macromol., vol. 171, pp. 44-58, 2021, doi: 10.1016/j.ijbiomac.2020.12.162. https://doi.org/10.1016/j.ijbiomac.2020.12.162
[4] Ansari, Shoeb Anwar Mohammed Khawja, et al. 'Magnetic iron oxide NPs: synthesis, characterization and functionalization for biomedical applications in the central nervous system.' Materials 12.3 (2019): 465." https://doi.org/10.3390/ma12030465
[5] NI, Dadfar SM Roemhild K. Drude, and S. Knüchel R. von Stillfried. 'Kiessling F. Lammers T.' Adv. Drug Delivery Rev 138 (2019): 302-325.," p. 5. https://doi.org/10.1016/j.addr.2019.01.005
[6] Buch, Pranali J., Yunrong Chai, and Edgar D. Goluch. 'Treating polymicrobial infections in chronic diabetic wounds.' Clinical microbiology reviews 32.2 (2019): e00091-18.," p. 6. https://doi.org/10.1128/CMR.00091-18
[7] Moskvin, Maksym, et al. 'Cerium oxide-decorated γ-Fe2O3 NPs: Design, synthesis and in vivo effects on parameters of oxidative stress.' Frontiers in Chemistry 8 (2020): 682," p. 7. https://doi.org/10.3389/fchem.2020.00682
[8] Noruozi, Abbas, and Alireza Nezamzadeh-Ejhieh. 'Preparation, characterization, and investigation of the catalytic property of α-Fe2O3-ZnO NPs in the photodegradation and mineralization of methylene blue.' Chemical Physics Letters 752 (2020): 137," p. 8. https://doi.org/10.1016/j.cplett.2020.137587
[9] Ali, Lamiaa MA, et al. 'Effect of superparamagnetic iron oxide NPs on glucose homeostasis on type 2 diabetes experimental model.' Life Sciences 245 (2020): 117361," p. 9. https://doi.org/10.1016/j.lfs.2020.117361
[10] Cho, NH1, et al. 'IDF Diabetes Atlas: Global estimates of diabetes prevalence for 2017 and projections for 2045.' Diabetes research and clinical practice 138 (2018): 271-281," p. 10. https://doi.org/10.1016/j.diabres.2018.02.023
[11] G. Abbas, K. B. Singh, N. Kumar, A. Shukla, D. Kumar, and G. Pandey, "Efficient anticarcinogenic activity of α-Fe2O3 NPs: In-vitro and computational study on human renal carcinoma cells HEK-293," Mater. Today Commun., vol. 26, no. January, p. 102175, 2021. https://doi.org/10.1016/j.mtcomm.2021.102175
[12] B. L. Tan, M. E. Norhaizan, W. P. P. Liew, and H. S. Rahman, "Antioxidant and oxidative stress: A mutual interplay in age-related diseases," Front. Pharmacol., vol. 9, no. OCT, pp. 1-28, 2018. https://doi.org/10.3389/fphar.2018.01162
[13] S. P. Wong, L. P. Leong, and J. H. William Koh, "Antioxidant activities of aqueous extracts of selected plants," Food Chem., vol. 99, no. 4, pp. 775-783, 2006. https://doi.org/10.1016/j.foodchem.2005.07.058
[14] A. Haider et al., "Green Synthesized Phytochemically (Zingiber officinale and Allium sativum) Reduced Nickel Oxide NPs Confirmed Bactericidal and Catalytic Potential," Nanoscale Res. Lett., vol. 15, no. 1, 2020. https://doi.org/10.1186/s11671-020-3283-5
[15] E. Paulson and M. Jothibas, "Significance of thermal interfacing in hematite (α-Fe2O3) NPs synthesized by sol-gel method and its characteristics properties," Surfaces and Interfaces, vol. 26, no. September, p. 101432, 2021. https://doi.org/10.1016/j.surfin.2021.101432
[16] H. I. Abdulah, A. M. Farhan, and A. J. Ali, "Photo-synthesis of nanosized α - Fe2O3 Available online www.jocpr.com," no. May, pp. 5-9, 2019.
[17] Dash, Priyanka, et al. 'Harnessing the biomedical properties of ferromagnetic α-Fe2O3 NPs with a plausible formation mechanism.' Ceramics International 46.16 (2020): 26190-26204.." https://doi.org/10.1016/j.ceramint.2020.07.117
[18] N. Abdul-Ameer Aboud, W. M. S. Alkayat, D. H. Hussain, and A. M. Rheima, "A comparative study of ZnO, CuO and a binary mixture of ZnO0.5-CuO0.5with nano-dye on the efficiency of the dye-sensitized solar cell," J. Phys. Conf. Ser., vol. 1664, no. 1, pp. 0-16, 2020. https://doi.org/10.1088/1742-6596/1664/1/012094
[19] Hollis, R. L., S. Salcudean, and D. W. Abraham. 'Toward a tele-nanorobotic manipulation system with atomic scale force feedback and motion resolution.' IEEE Proceedings on Micro Electro Mechanical Systems, An Investigation of Micro Structures, Sensors, Ac," p. 15.
[20] Huang, Wei, et al. 'Microwave assisted crystalline and morphology evolution of flower-like Fe2O3@ iron doped K-birnessite composite and its application for lithium ion storage.' Applied Surface Science 525 (2020): 146513," p. 18. https://doi.org/10.1016/j.apsusc.2020.146513
[21] Samrot, Antony V., et al. 'Azadirachta indica influenced biosynthesis of super-paramagnetic iron-oxide NPs and their applications in tannery water treatment and X-ray imaging.' Journal of Nanostructure in Chemistry 8.3 (2018): 343-351.," p. 19. https://doi.org/10.1007/s40097-018-0279-0
[22] Kumar, M. Suresh Chandra, V. Selvam, and M. Vadivel. 'Synthesis and characterization of silane modified iron (III) oxide NPs reinforced chitosan nanocomposites.' Engineering Science & Advanced Technology 2 (2012): 1258-1263.."
[23] Saqib, Saddam, et al. 'Synthesis, characterization and use of iron oxide nano particles for antibacterial activity.' Microscopy research and technique 82.4 (2019): 415-420." https://doi.org/10.1002/jemt.23182
[24] Ali, Musrat, et al. 'Scanning electron microscopy of bio-fabricated Fe2O3 NPs and their application to control brown rot of citrus.' Microscopy Research and

Technique 84.1 (2021): 101-110.." https://doi.org/10.1002/jemt.23570

[25] Jin, Ying, et al. 'Synthesis of unit-cell-thick α-Fe2O3 nanosheets and their transformation to γ-Fe2O3 nanosheets with enhanced LIB performances.' Chemical Engineering Journal 326 (2017): 292-297." https://doi.org/10.1016/j.cej.2017.05.155

[26] P. N. V. K. Pallela et al., "Antibacterial efficacy of green synthesized α-Fe2O3 NPs using Sida cordifolia plant extract," Heliyon, vol. 5, no. 11, p. e02765, 2019, doi: 10.1016/j.heliyon.2019.e02765. https://doi.org/10.1016/j.heliyon.2019.e02765

[27] Hashim, Fouad Sh, et al. 'Photocatalytic degradation of GRL dye from aqueous solutions in the presence of ZnO/Fe2O3 nanocomposites.' Composites Communications 16 (2019): 111-116.." https://doi.org/10.1016/j.coco.2019.09.008

[28] Medhe, Sharad, Prachi Bansal, and Man Mohan Srivastava. 'Enhanced antioxidant activity of gold nanoparticle embedded 3, 6-dihydroxyflavone: a combinational study.' Applied Nanoscience 4.2 (2014): 153-161.." https://doi.org/10.1007/s13204-012-0182-9

[29] W. Ahmad, V. Singh, S. Ahmed, and M. Nur-e-Alam, "A comprehensive study on antibacterial antioxidant and photocatalytic activity of achyranthes aspera mediated biosynthesized Fe2O3 NPs," Results Eng., vol. 14, no. April, p. 100450, 2022. https://doi.org/10.1016/j.rineng.2022.100450

[30] M. Harshiny, C. N. Iswarya, and M. Matheswaran, "Biogenic synthesis of iron NPs using Amaranthus dubius leaf extract as a reducing agent," Powder Technol., vol. 286, pp. 744-749, 2015, https://doi.org/10.1016/j.powtec.2015.09.021

[31] J. Xiu, Y. Zhang, B. Ahamad, and A. Gulnaz, "Facile preparation of Fe2O3 NPs mediated by Centaurea alba extract and assessment of the anti-atherosclerotic properties," Arab. J. Chem., vol. 15, no. 1, p. 103493, 2022. https://doi.org/10.1016/j.arabjc.2021.103493

How to Cite

D. H. Hilo, A. H. Ismail, and Z. S. Al-Garawi, “Green Synthesis of A-Fe2O3 from Ginger Extract Enhanced the Potential Antioxidant Activity Against DPPH”, *Al-Mustansiriyah Journal of Science*, vol. 33, no. 4, pp. 64–71, Dec. 2022.